LANGMUIR

pubs.acs.org/Langmuir Article

Probing the Interfacial Properties of Oil−Water Interfaces Decorated with Ionizable, pH Responsive Silica Nanoparticles

Ahmed Wasel Alsmaeil, Antonios Kouloumpis, Georgia Potsi, Mohamed Amen Hammami, Mazen Yousef Kanj, and Emmanuel P. Giannelis*

Cite This: *Langmuir* 2023, 39, 3118−3130 Read Online

ACCESS | Metrics & More | Article Recommendations | SI Supporting Information

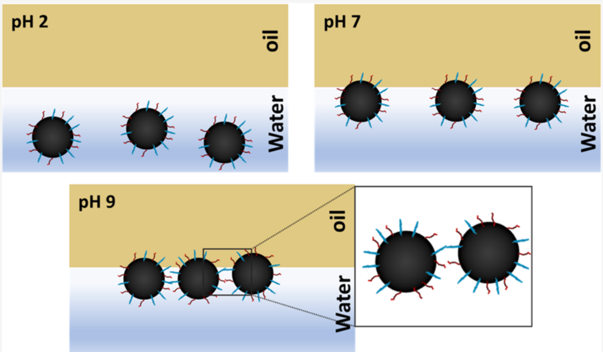

ABSTRACT: Particle-stabilized emulsions (Pickering emulsions) have recently attracted significant attention in scientific studies and for technological applications. The interest stems from the ease of directly assembling the particles at interfaces and modulating the interfacial properties. In this paper, we demonstrate the formation of stable, practical emulsions leveraging the assembly of ionizable, pH responsive silica nanoparticles, surface-functionalized by a mixture of silanes containing amine/ammonium groups, which renders them positively charged. Using pH as the trigger, the assembly and the behavior of the emulsion are controlled by modulating the charges of the functional groups of the nanoparticle and the oil (crude oil). In addition to their tunable charge, the particular combination of silane coupling agents leads to stable particle dispersions, which is critical for practical applications. Atomic force microscopy and interfacial tension (IFT) measurements are used to monitor the assembly, which is controlled by both the electrostatic interactions between the particles and oil and the interparticle interactions, both of which are modulated by pH. Under acidic conditions, when the surfaces of the oil and the nanoparticles (NPs) are positively charged, the NPs are not attracted at the interface and there is no significant reduction in the IFT. In contrast, under basic conditions in which the oil carries a high negative charge and the amine groups on the silica are deprotonated while still positively charged because of the ammonium groups, the NPs assemble at the interface in a closely packed configuration yielding a jammed state with a high dilatational modulus. As a result, two oil droplets do not coalesce even when pushed against each other and the emulsion stability improves significantly. The study provides new insights into the directed assembly of nanoparticles at fluid interfaces relevant to several applications, including environmental remediation, catalysis, drug delivery, food technology, and oil recovery.

■ INTRODUCTION

The assembly of nanoparticles at the oil−water interface has received widespread attention and has been extensively studied by numerous investigators. These studies include but are not limited to food processing and production,[1−3] drug encapsulation,[4,5] environmental remediation,[6−8] and enhanced oil recovery.[9−14] The interest stems from the fact that particle-laden interfaces offer a route to controlled interfacial properties, including the ultimate stability of an emulsion.[15−19] Oil droplets surrounded by particles result in improved viscoelastic properties of the interface. Hence, emulsion breakup, coalescence, or coarsening can be circumvented or slowed.[1,20−22]

Spontaneous adsorption of nanoparticles (NPs) at the oil−water interface is driven by the decrease in the free energy of the oil−water interface, which is given by[23,24]

$$\Delta E = -\frac{\pi d^2}{4\gamma_{\mathrm{OW}}}[\gamma_{\mathrm{OW}} - (\gamma_{\mathrm{PW}} - \gamma_{\mathrm{PO}})]^2 \tag{1}$$

where d is the particle diameter and γ_{OW}, γ_{PW}, and γ_{PO} are the interfacial tension of oil−water, particle−water, and particle−oil interfaces, respectively. Using the Young−Laplace equation, eq 1 could be written as follows:[23−26]

$$\Delta E = -\frac{\pi d^2}{4}\gamma_{\mathrm{OW}}(1 - |\cos\theta_{\mathrm{OW}}|)^2 \tag{2}$$

where θ_{OW} is the contact angle of the particles at the oil−water interface measured from the aqueous phase.[26,27] The adsorption energy of chemically homogeneous nanoparticles at the interface is directly proportional to the particle diameter and the contact angle the particle makes at the interface. The maximum adsorption at a constant size and interfacial tension

Received: December 4, 2022
Revised: February 7, 2023
Published: February 15, 2023

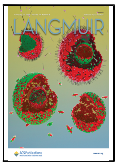

ACS Publications

https://doi.org/10.1021/acs.langmuir.2c03286

happens when the contact angle is 90°, that is for particles with equal wettability for both the oil and water phases.[28] Moreover, the size plays a major role in the stabilization of particles at the interface. For micrometer-sized particles, the adsorption energy could be orders of magnitude larger than the thermal energy of the system; i.e., $|\Delta E| \gg 10^6\ kT$ (k is the Boltzmann constant, and T is the temperature in kelvin), which results in the particles being trapped at the interface. For nanosized particles, the adsorption energy is smaller but still large compared to that of the thermal fluctuations (e.g., ~2500 kT for a 10 nm particle with a 90° contact angle) in the system and thus sufficient to immobilize the NPs.[24,29−31] Hence, while nanoparticles do not adsorb as strongly at oil−water interfaces compared to micrometer-sized particles, they still form a "solid-like" assembly at the interface.[24,32] This behavior distinguishes nanoparticles from molecular surfactants, which are more dynamic and can be easily detached from the interface.

Common strategies for enhancing the adsorption of NPs at the oil−water interface and improving emulsion stability involve surface modification of NPs by surfactants or polymers or controlling the properties of the aqueous phase, including its pH and ionic strength.[25,33−39] For example, Biswal et al. studied the effects of utilizing anionic, cationic, and nonionic surfactants in the adsorption of 0.1 wt % silica NPs at the hexane−water interface. They observed that the interfacial tension did not change from that of the pristine oil−water interface, when using the NPs alone. In contrast, when sodium dodecyl sulfate (SDS) or cetyltrimethylammonium bromide (CTAB) was used, the IFT was reduced from 49 mN/m (pristine interface) to ~25 and ~35 mN/m for SDS and CTAB, respectively.[33] Moreover, Anjali et al. investigated using hematite particles in stabilizing oil-in-water emulsions. The stability was strongly dependent on pH. Specifically, under close to neutral conditions (pH 6.5), a closed-packed assembly of the particles at the *n*-decane−water interface was formed, resulting in a stable emulsion. However, the emulsion was destabilized when the pH was changed to either 2 or 12.[37]

The presence of salts in the aqueous phase is another key factor that affects the assembly of NPs at liquid−liquid interfaces. Chain et al. studied the effects of ionic strength on the assembly and packing of silica NPs functionalized with carboxylic acid groups. The particles formed a closed-packed assembly and transformed the liquid-like to a solid-like interface, when NaCl was present in the aqueous phase.[38] Similarly, the assembly of negatively charged nanocellulose particles at the soybean oil−water interface depended on whether NaCl was present. The NaCl screened the electrostatic repulsion between the suspension and the oil, which resulted in the accumulation and jamming of the nanoparticles at the interface. Under these conditions, the interface behaved like a solid film.[39]

Another promising approach is based on introducing and modulating the electrostatic interactions between particles and oil, for example, by dissolving oil-soluble surfactants into the oil phase and having oppositely charged NPs in the aqueous phase. The strong interaction between the NPs and the complementary polar groups in oil results in interfacial jamming of the NPs at the interface.[29,38,40] For instance, addition of NH_2-polydimethylsiloxane (PDMS) to the oil phase results in adsorption of COOH-functionalized NPs at the water−toluene interface. The preferential assembly by the negatively charged particles and the positively charged groups in the oil reduced the IFT between the two liquids. Moreover, the modulus of the interface increased as a result of the assembly of the NPs.[41] The strong electrostatic interactions resulted in the long-term stability of oil droplets even in a non-equilibrium shape.[42] In the same framework, Sun et al. controlled the assembly of graphene oxide (GO) at the toluene−water interface and found that the oil−water interface buckled and reached a jamming state, due to polar and ionizable groups in the system.[43]

The previous studies provided several examples of model systems and how electrostatic interactions played a major role in the assembly of NPs. However, these studies typically neglect the stability of the NPs under different conditions, a feature critical for practical applications. In addition, they rarely discuss the importance of interparticle interactions compared to those between the particles and the oil. In this work, we demonstrate that we can modulate both the particle−oil and interparticle interactions by changing the pH of the aqueous phase to direct the particle assembly. The work provides new insights into our understanding of the stability of emulsions facilitated by the addition of NPs. In addition, by expanding the work to nonmodel systems and by using NP systems with excellent colloidal stability under different conditions, we provide further evidence that these concepts are directly applicable and can be exploited in real applications.

Specifically, we demonstrate dramatic increases in stability of a crude oil-in-water emulsion using ionizable, pH responsive silica nanoparticles. The silica nanoparticles are functionalized by blending two types of silanes: one containing quaternary ammonium and the other containing both primary and secondary amine groups. By their nature, the quaternary ammonium groups are permanently positively charged, while the charge on the primary and secondary amine groups is modulated by changing the pH of the aqueous phase. The combination of permanently charged groups and other surface groups, where charges are developed in response to pH, provides an easy and consistent way to control the overall amount of charge on the NPs. As a result, in addition to the control of the interactions between the particles and the oil phase, the interparticle interactions can be fine-tuned. Another advantage of our approach is that the particular combination of silane coupling agents leads to stable particle dispersions at different pHs. Altogether, this work represents the first systematic study combining both microscopic and macroscopic analytical techniques and provides new insights into the underlying mechanism of particle assembly at liquid−liquid interfaces. We note that another trigger for modulating interactions is ionic strength using various electrolytes, and we plan to communicate these results in a forthcoming publication.

EXPERIMENTAL SECTION

Materials. LUDOX HS-30 colloidal silica (30 wt % in water) with an average diameter of 13 nm, N1-(3-trimethoxysilylpropyl)-diethylenetriamine (TMPA), hydrochloric acid (37%), and CTAB were purchased from Sigma-Aldrich and used without further purification. The 4 nm colloidal silica (15 wt % in water) was purchased from Fisher Scientific and used without further purification. *N*-Trimethoxysilylpropyl-*N*,*N*,*N*-trimethylammonium chloride (TMAC) was obtained from Gelest. Sodium hydroxide pellets (98%) were purchased from Alfa Aesar. Crude oil (density of 0.82 g/mL, viscosity of 6.1 mPa s) was obtained from the Cornell Energy Systems Institute. The oil composition is 33.1% saturates, 47.3% aromatics, 8.7% resins (polars I), and 10.9% asphaltenes (polars II) determined by SARA (saturates, aromatics, resins, and asphaltene)

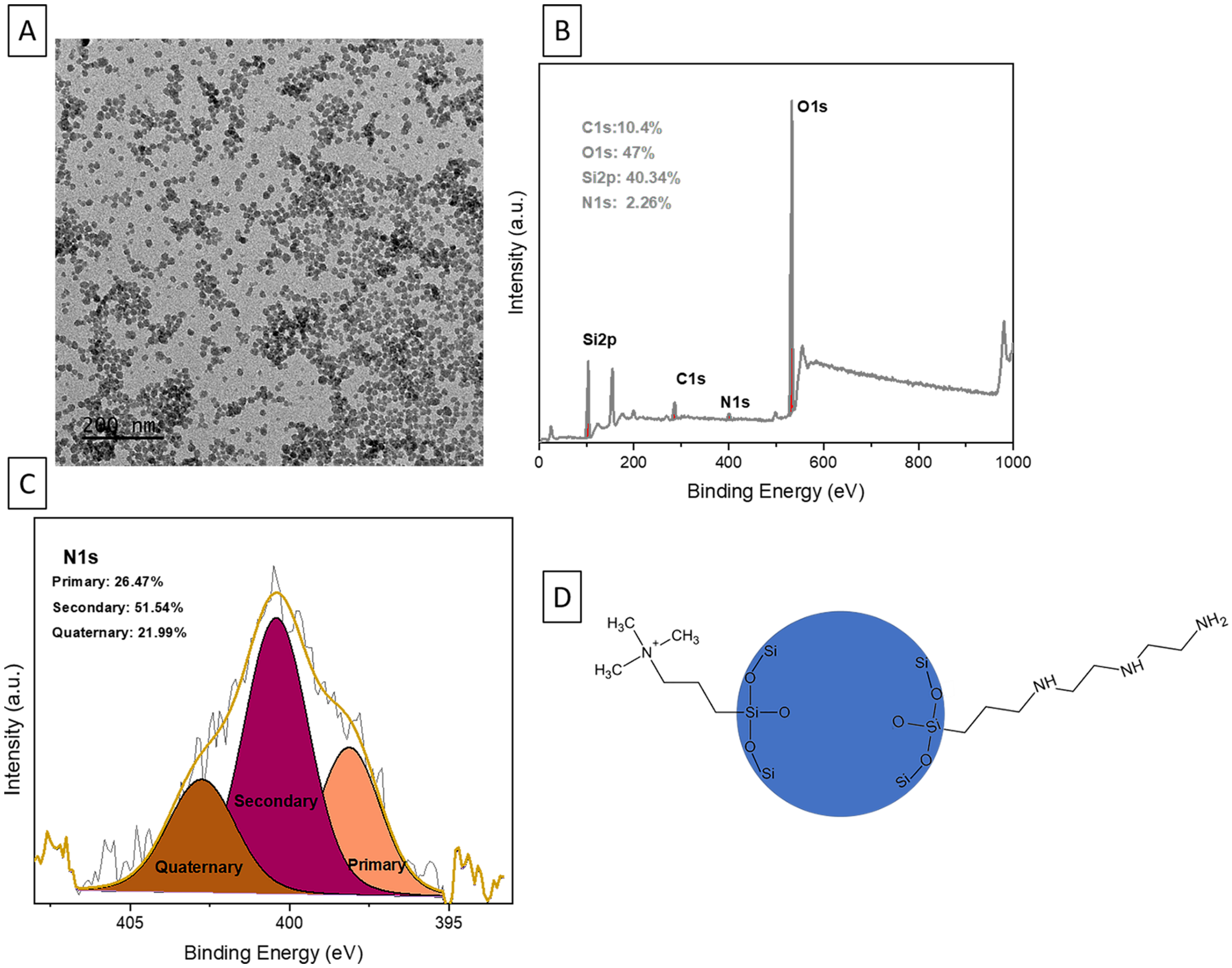

Figure 1. (A) TEM image of the silane-modified silica NPs showing a spherical morphology. (B) XPS survey spectrum. (C) High-resolution spectrum for N 1s. (D) Schematic showing the surface chemistry of the modified silica NPs. The scale bar in panel A is 200 nm.

analysis. Hexadecane used in some experiments to dilute the crude oil was purchased from Sigma-Aldrich.

Surface Functionalization of Silica NPs. The double functionalization of the silica NPs was carried out utilizing a 1:1 mixture of TMPA and TMAC. In brief, 3 g of TMAC and 1.5 g of TMPA were added to 30 mL of deionized (DI) water. The solution was stirred for 30 min at room temperature. Then a dispersion of 9 g of colloidal silica NPs (13 nm) in 150 mL of DI water that had been sonicated previously for 1 h was added dropwise to the solution. The mixture was then transferred to an oil bath at 70 °C and kept stirring overnight. The reaction product was transferred to a dialysis apparatus and kept for 7 days immersed in a water bath at pH 4 to prevent the formation of a gel in the buffer solution. The pH was maintained at 4 by adding aliquots of 0.1 M HCl or 0.1 M NaOH as needed. A similar protocol was followed for the functionalization of the 4 nm silica NPs with the exception that 18 g of the silica dispersion was used.

Analytical Characterization and Methods. The ζ potential was determined at 25 °C using the Zetasizer ZS90 (Malvern Instruments Ltd.) and Malvern polycarbonate folded capillary cells (DTS1070) with backscattering detection at 173°. The samples were allowed to equilibrate in the instrument chamber for 120 s prior to measurement. The suspension (1 wt %) was sonicated for 30 min before each measurement using a water bath sonicator. For measurements of the oil–water mixtures, the pH of DI water was first adjusted with 0.1 M NaOH or 0.1 M HCl. Then, 0.3 mL of oil was added to 2.7 mL of water. The emulsions were prepared with an ultrasonicator (Fisher Scientific, Q500) at 10% amplitude for 10 min. Ultrasonication was used to enhance the stability of emulsions and improve the reproducibility of the measurements.[44] The average of three independent measurements of each system is reported.

The stability of the particles at different pHs was determined using a dispersion analyzer (LUMiSizer 651 by LUM Gmbh). First, 0.4 mL of a 1 wt % suspension was added to a cell (polyamide cells, 2 mm path length), and the samples were subjected to a centrifugation acceleration of 520$\vec{g}$ for 8 min. The detector was operated at a wavelength of 410 nm. For the oil-in-water emulsions, samples were prepared by adding 0.3 mL of oil to 2.7 mL of an aqueous suspension at different pHs. The mixture was homogenized at 10 000 rpm for 30 min using an IKA Ultra-Turrax T-25 instrument with an 8 mm dispersion tool. The stability of the emulsions was studied at 120$\vec{g}$. Transmission profiles were collected every 20 s. For the sake of clarity, transmission spectra are colored first red at the beginning and then green as time progresses. Because the emulsions are opaque, the detector was operated at a wavelength of 870 nm. The changes in the transmission spectra with time and position were recorded and used to determine the stability of the suspension as reported previously.[45−48] SEPView software (LUM, GmbH) was used to calculate the instability (separation) indices. The separation index is used to monitor the sedimentation or creaming of the suspension with time. The separation index quantifies the changes and is defined as the transmission of the system at time t divided by the maximum

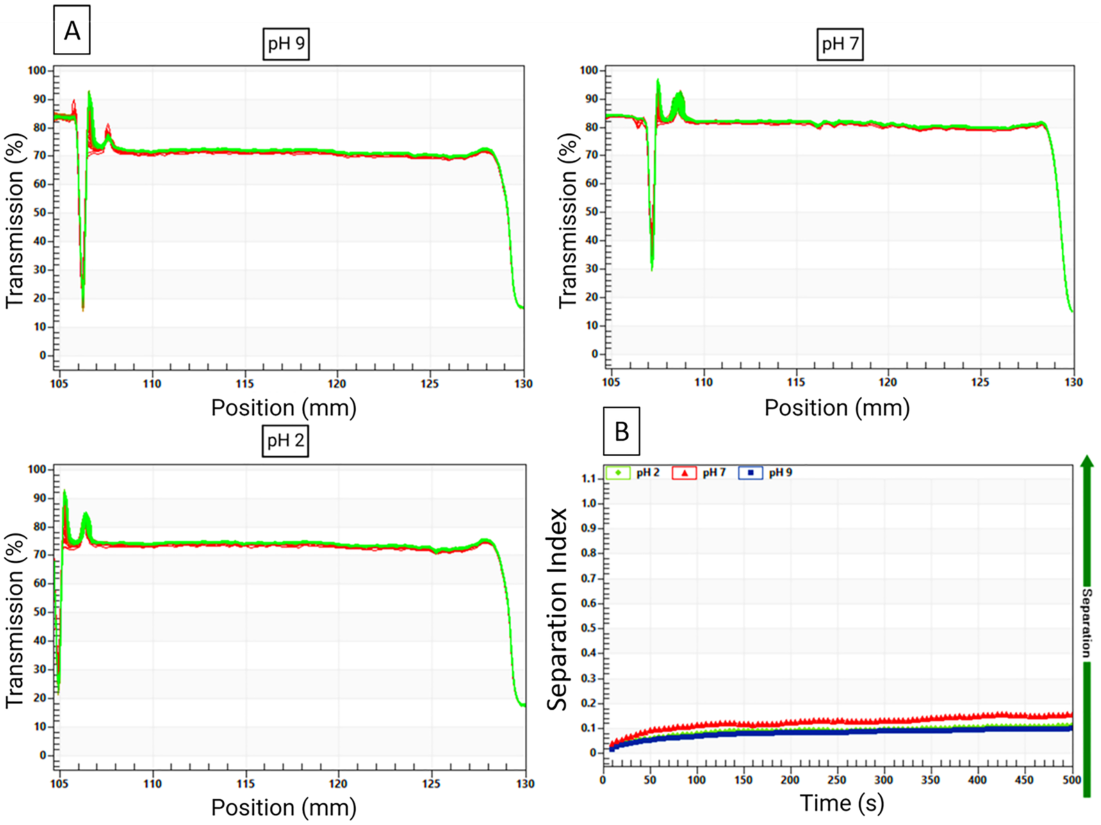

Figure 2. (A) Accelerated tests at $520\vec{g}$ of 1 wt % NPs at different pHs. (B) Separation index for the different pHs studied. The color in the transmission spectra changes from red to green as the accelerated separation experiment progresses.

transmission. Its value ranges from 0 to 1, where 0 corresponds to no separation and 1 indicates complete separation.[49]

The morphology and size of the particles were studied using transmission electron microscopy (TEM) (FEI-Tecnai 12 BioTwin TEM, FEI Co., Hillsboro, OR) with an LaB6 electron source at 120 kV using a Gatan Orius S1000 CCD camera. A 1 wt % suspension in water was placed on a carbon-coated copper grid prior to imaging. The particle size distribution was analyzed using ImageJ.

X-ray photoelectron spectroscopy (XPS) was performed using an ESCA 2SR XPS instrument equipped with an Al Ka 1486.7 eV monochromator and an operating pressure of 10^{-9} Torr. The samples in powder form were deposited on copper tape. Survey and high-resolution spectra were collected at pass energies of 200 and 50 eV, respectively. Acquired spectra were corrected using the C 1s core level region as a reference.

The interfacial tension and dilatational modulus were measured using a Spinning Drop Tensiometer (SDT, KRÜSS). An oil droplet was injected into a capillary tube with an inner diameter of 3.25 mm and rotated at a fixed speed. The rotational speed was set at 10 000 rpm for all experiments. The oil droplet shape was fitted to the Young−Laplace equation to determine the IFT.[50] In the early stages of the experiment, the IFT decreased continuously as the droplet rotated and it reached a plateau after some time (the plateau value is defined as the equilibrium IFT). When the equilibrium IFT was reached, the drop was disturbed sinusoidally at a frequency of 0.1 Hz. The area of the oil droplet was determined using MATLAB (R2018b). The changes in the area of the droplet and the IFT were used to calculate the complex dilatational modulus using the following equation:[16,20,51]

$$E = A\frac{\partial \gamma}{\partial A} \tag{3}$$

where A is the surface area of the droplet.

The amplitude of oscillation was maintained at 1000 rpm so that the changes in area are small (<10%) and the response is kept linear. An example of the response of the interfacial layer to the sinusoidal changes of the rotational speed is shown in Figure S1. The scaled surface area shown in Figure S1 and discussed in the experiment is defined as the surface area of the oil droplet at any time of the experiment divided by the maximum surface area of the oil droplet at the end of the experiment (when the IFT reaches the equilibrium value). The increase in the surface area is the difference between the maximum and minimum area divided by the maximum area. Further information about the spinning drop technique for studying oil−water interfacial rheology is provided elsewhere.[51]

Atomic force microscopy (AFM) experiments were conducted in peak force tapping mode on a Multimode 8, Nanoscope 6, using Peakforce-HIRS-F-A cantilevers and a fluid cell. The deflection sensitivity of the photodetector was calibrated by acquiring approach−retract curves on a fused silica sample in oil. The spring constant of the cantilever was calibrated by the thermal method. A small droplet of the aqueous solution with or without the NPs was placed on a silicon wafer (p-type Si doped with boron, single side polished, purchased from Pure Wafer), and a larger drop of oil was added to completely cover the water droplet.[52,53] To facilitate imaging of the interface, the oil was diluted with hexadecane (25:75 $V_{\text{hexadecane}}$:V_{oil}) to make the sample more transparent. Note that the IFT and modulus of the diluted samples are similar to those of the undiluted oil.

A Zeiss LSM 710 confocal laser scanning microscope with a Plan-Apochromat 10×, 1.4 water-immersion objective was used to study the emulsions. Equal volumes of oil and a 1 wt % suspension of silica NPs in water were prepared with a protocol similar to that of the LUMiSizer experiments. Approximately 100 μL of the emulsion was poured onto a glass slide and covered with a coverslip. No addition of fluorescent dyes was necessary because of the autofluorescence of the oil.[10]

https://doi.org/10.1021/acs.langmuir.2c03286

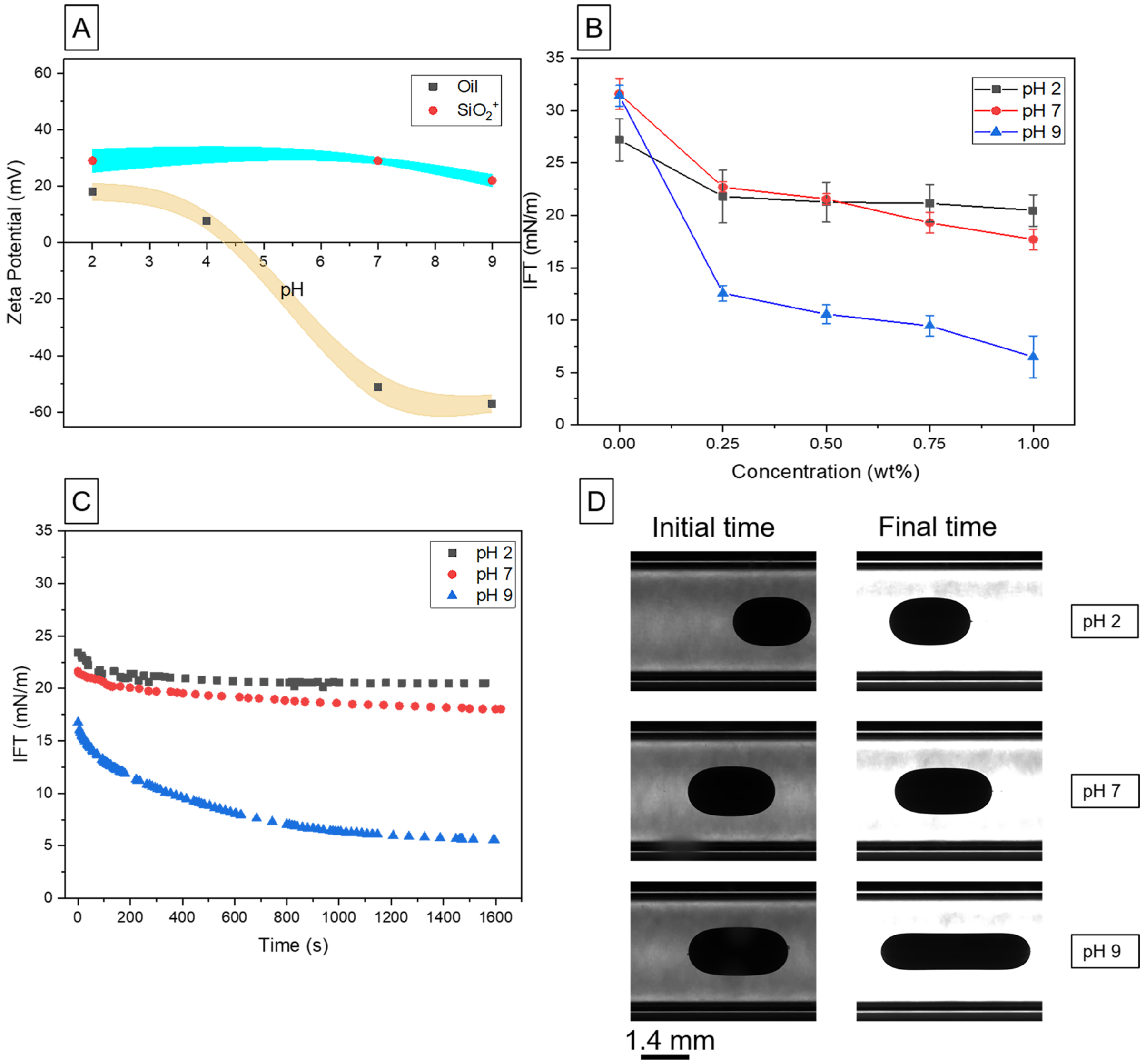

Figure 3. (A) ζ potentials of crude oil and the modified silica NPs at different pHs (the color shadow in panel A indicates the error range of the measurements). (B) IFT for oil−water mixtures as a function of the concentration of NPs at different pHs. (C) Dynamic IFT for 1 wt % NPs at different pHs: 2 (black), 7 (red), and 9 (blue). (D) Comparison of the oil droplet shape at the initial time and final time at different pHs.

■ RESULTS AND DISCUSSION

Characterization of the Surface-Modified Colloidal Silica NPs. The morphology and size of the NPs were first characterized by TEM. The functionalized NPs have a spherical shape with an average diameter of ∼15 ± 3 nm (Figure 1A), determined by analyzing 100 NPs. Surface functionalization of the silica NPs with the mixture of silanes was confirmed by XPS. The presence of the nitrogen N 1s and carbon C 1s peaks in the wide scan survey (Figure 1B) confirms the attachment of the silanes onto the silica NPs. To further characterize the type of nitrogen species, deconvolution of the high-resolution scan of the N 1s core level region was used. As shown in Figure 1C, the peaks around 398, 401, and 402.5 eV correspond to three distinct types of amines: primary, secondary, and quaternary, respectively, in a ratio of 1:0.51:0.43.[54,55] This ratio is consistent with the composition of the silanes used for the functionalization, confirming that for each quaternary ammonium and primary amine present (from TMAC and TMPA, respectively) on the surface of the particles, there are two secondary amines (from TMPA) as illustrated in Figure 1D.

To further confirm the surface functionalization of the NPs, the ζ potential of both modified and unmodified particles at pH 7 was measured (Figure S2). The unmodified particles have a ζ potential of −25 ± 2 mV, whereas the modified particles show a ζ potential of 30 ± 1.5 mV. The positively charged surface is due to the presence of the quaternary ammoniums, which are permanently charged irrespective of the pH of the medium (as well as the primary and secondary alkylamine groups, which are proton acceptors with a pK_a value of 9−11).[56,57] Hence, the primary and secondary amine groups are expected to be protonated at neutral pH and together with the quaternary ammonium result in an overall positively charged particle.

Colloidal Stability of the Modified Silica NPs. The colloidal stability of the particles was assessed at three different pHs (2, 7, and 9) using the dispersion analyzer. Specifically, space−time−extinction profiles (STEPs) were obtained while the samples were spun at 520$\vec{g}$. There are three possible scenarios of a suspension subjected to centrifugation. When the suspension is stable, the transmittance remains constant as a function of time over the entire length of the cell. In contrast, when sedimentation takes place, the transmittance increases with time at the top and decreases at the bottom of the cell following the particle redistribution. Finally, a suspension in which the transmittance is reduced at the top of the cell and increases at the bottom is representative of creaming.

Figure 2A shows the temporal evolution of the transmission profiles for the suspension of SiO_2^+ NPs at different pHs. Even when an aggressive centrifugation acceleration of $520\vec{g}$ was used, the particles did not sediment as evidenced by the almost unchanged transmission profiles and the absence of a sedimentation layer forming at the bottom of the sample. The separation index (calculated as stated in the Experimental Section) for the three systems did not exceed 0.1, effectively indicating that the NP suspension is stable even under these extreme, accelerated testing conditions (Figure 2B). We attribute the stability of the suspension to a combination of electrostatic and steric stabilization. The high positive ζ potential (high charge) of the particles, irrespective of the pH, helps prevent aggregation. In addition, the silanes form a corona around the particles preventing close contact of the particles.[58,59] We also note that both the small size and the relatively low density of the particles are contributing to their stability.

Interfacial Activity of the Positively Charged Particles. Figure 3A summarizes the ζ potential of a 1 wt % aqueous suspension of the silica particles and a 10% by volume oil-in-water emulsion at different pHs. The NPs are always positively charged regardless of the pH due to the presence of the quaternary ammonium groups on the surface. The ζ potential is 30 mV at both pH 2 and 7 and reaches 22 mV at pH 9. In addition to the quaternary ammonium groups, the primary and secondary amines are protonated at pH 2 and 7 and contribute to the positive ζ potential. At pH 9, the primary and secondary amines are mostly deprotonated, resulting in a decrease in the ζ potential, which is due largely to the quaternary ammonium groups.[56,57] The oil−water mixture, on the contrary, shows two distinct regimes. At pH 2, it is positively charged, and it becomes negatively charged at pH 7 and 9. It is well established that crude oil contains various polar groups, including carboxylic acid that segregate at the interface, when mixed with water. The presence of carboxylic groups was confirmed by Fourier transform infrared (FT-IR) spectroscopy by comparing the spectra of crude oil and hexadecane containing 1 wt % stearic acid (Figure S3).[60,61] Carboxylic acid groups have a pK_a value in the range of 4−5, and hence, below this pH, the surface groups are protonated; the carboxylic groups are deprotonated above pH 4−5, and the surface becomes negatively charged.[62,63] We note that the origin of the charge in crude oil−water mixtures is different from that in pure hexadecane, which spontaneously develops a negative charge, when mixed with water.[64] The negative charge in crude oil is the result of the carboxylic groups present on the surface. They are responsible for attracting the positively charged silica NPs (see below). In contrast, hexadecane does not interact with the silica NPs and the properties of the interface are largely unaffected as described below.

As stated above, the NPs were designed to be positively charged so that they are complementary to the negatively charged crude oil. As such, they assemble at the oil−water interface driven by electrostatic interactions between the particles and the oil. In the following, we systematically probe the assembly and interfacial behavior starting by first examining the effect of the nanoparticles on the IFT as a function of pH.

Figure 3B shows the IFT values for oil−water mixtures in the presence of the silica NPs at different pHs and NP concentrations. In all cases, the IFT decreased significantly in the presence of NPs. While there appears to be a weak dependence on NP concentration in the aqueous phase (0.25−1.00 wt %) (higher concentrations lead to lower IFT values), there is a much stronger dependence on pH. At pH 9, the IFT decreases significantly from the pristine oil−water IFT of 32 to 13 mN/m, when 0.25 wt % of NPs is added; the lowest IFT was achieved at 1 wt % NPs showing a value of 5.5 mN/m. Note that at pH 9 the surface charge of oil becomes more negative (−57 mV) and that of the particles less positive (22 mV) compared to those at neutral or acidic pHs.

The dynamic IFTs with the corresponding changes in the area of the oil droplet for a 1 wt % NP suspension at different pHs are shown in panels C and D of Figure 3. At pH 2, the interfacial tension reaches an equilibrium value of 20.5 mN/m in a very short time, indicating a weak adsorption at the interface (which will be discussed in more detail below) because the electrostatic interactions are not favorable (both the oil and the particles are positively charged). At pH 7, the IFT reaches an equilibrium value of ∼18 mN/m. At both pH 2 and 7, the IFT exhibits similar behavior at the beginning until ∼300 s. In contrast, at pH 9, due to the strong electrostatic attraction and the preferential adsorption of the particles at the interface, the IFT is reduced from 32 mN/m [pristine oil−water IFT (Figure 3B)] to 17 mN/m (Figure 3C) immediately. The reduction is so fast that the change exceeds the time-scale resolution of the instrument. The IFT then continues to decrease quickly to 10 mN/m in 500 s and then gradually until it reaches a value of ∼5.5 mN/m. For pH 2, both the particles and the oil are positively charged and the two repel each other so the adsorption is limited. Nevertheless, a small number of NPs is still present at the interface; the adsorption is facilitated by hydrogen bonding perhaps via a network of water molecules. At pH 7, the charges between the oil and the silica NPs become complementary, promoting adsorption and assembly at the interface. However, as we will note below, the interparticle interactions also play a significant role in the assembly preventing a dense layer of NPs and, hence, the reduction of the IFT at pH 7 is smaller. At pH 9, the conditions are optimal for a denser assembly and the value of IFT is reduced significantly. It is worth mentioning that the data for pH 9 can be separated into two time regimes. At the beginning, there is a linear relationship between the IFT and $\sqrt{t}$, suggesting that the process is diffusion-limited. Later, the IFT is proportional to $1/\sqrt{t}$, indicating the process is adsorption (reaction)-controlled. In contrast, at pH 7, the dynamic IFT shows a linear relationship with $\sqrt{t}$ for the entire process.[26,65]

The oil droplet behavior at a constant number of revolutions per minute in the presence of NPs at different pHs is shown in Figure 3D. The corresponding change in the surface area of the oil droplets is consistent with the IFT results. At pH 2, the increase in the area is relatively small. This behavior is similar to the changes in the oil surface area in DI water in the absence of NPs, where the increase is ∼2%. The surface area increases by 5% at pH 7. The corresponding change at pH 9 is ∼20%.

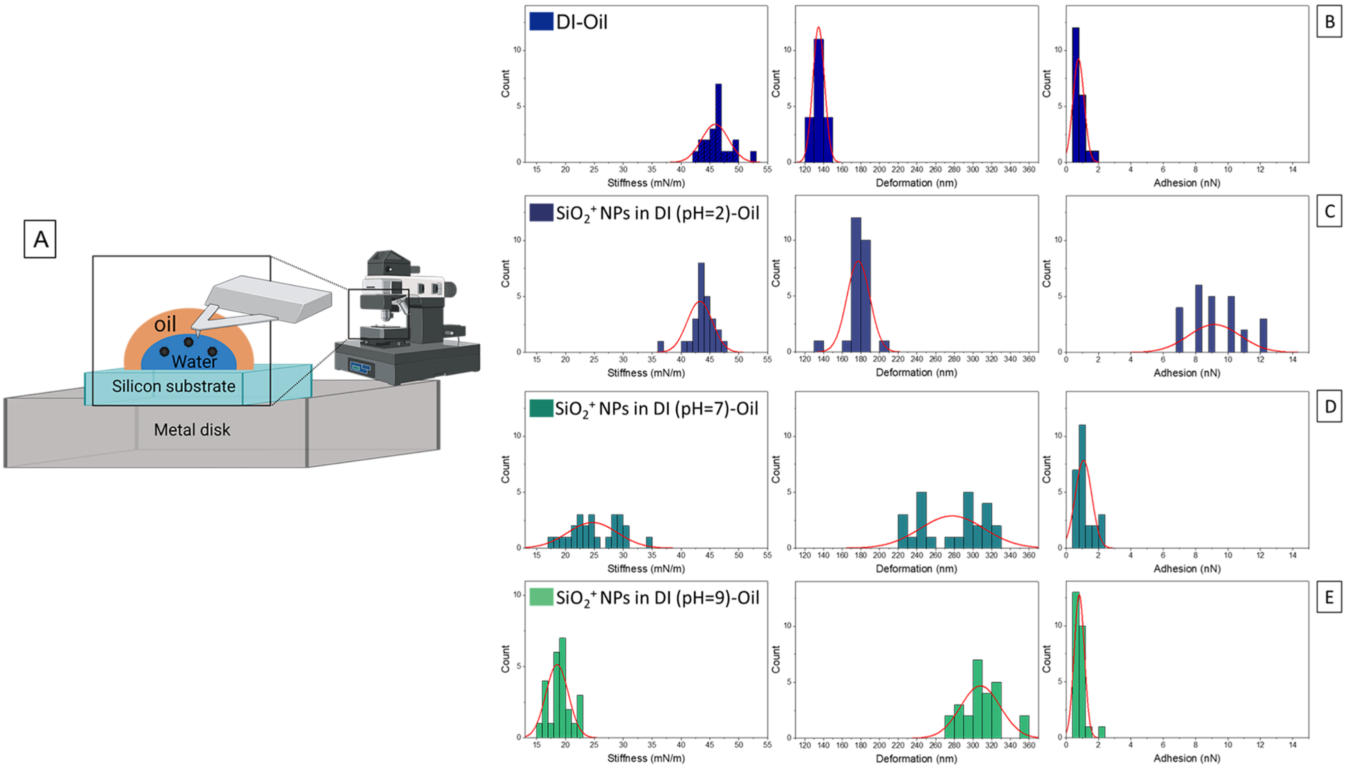

Figure 4. (A) Schematic representation of the AFM experiment. (B−E) Histograms of stiffness, deformation, and adhesion obtained from AFM force spectroscopy measurements: (B) oil−DI water in the absence of NPs (pH 7) and (C−E) oil−water in the presence of 1 wt % NPs with the pH adjusted to 2, 7, and 9, respectively. The solid lines in panels B−E are the normal distribution fits to the parameters measured by AFM.

These trends are consistent with the stronger adsorption and denser assembly of the NPs at the oil−water interface as the pH is increased.

The previous discussion focused on the macroscopic behavior based on the interfacial tension measurements. These results were supported by in situ, atomic force microscopy measurements at different pHs (Figure 4A). In addition to imaging, we used force spectroscopy measurements to provide information regarding the interfacial mechanical properties (i.e., deformation, stiffness, and adhesion of the interface) for the various systems (Figure 4B−E).

At pH 2 and in the presence of NPs, the deformation of the oil−water interface is slightly higher and the stiffness is slightly lower compared to those of the pristine oil−water interface. The interfacial area resists expansion and the creation of a new surface area because of the unfavorable interactions between the oil and water. The deformation increases from ∼170 ± 6 to ∼280 ± 12 nm when the pH is increased to 7. At pH 7, where the oil is negatively charged and the particles are positively charged, the attraction of NPs and the accompanying decrease in IFT make deformation of the interface more favorable. The highest deformation is at pH 9, where it increases to an average of ∼310 ± 34 nm. The trends observed are consistent with the results from the dynamic IFT measurements discussed above. Deformation is expected to increase with a decrease in interfacial tension, because it is energetically less demanding to create new surface area.[66,67] Stiffness is inversely proportional to deformation (i.e., high deformation indicates low stiffness, or lower resistance to form the interface). Accordingly, the stiffness is ∼18 ± 2 mN/m at pH 9, and it increases to 25 ± 4 mN/m at pH 7. The stiffness for the system at pH 2 is only marginally smaller than that in the absence of the nanoparticles (45 ± 2 mN/m).

In addition to stiffness and deformation, the force spectroscopy measurements provide information about the adhesion experienced by the AFM tip as it retracts from the interface. The mean interface adhesion force in the absence of NPs is 0.8 ± 0.3 nN. When NPs are introduced into the aqueous phase at pH 7 or 9, the adhesion does not change significantly (1 ± 0.5 nN at pH 7 and 0.8 ± 0.3 nN at pH 9), suggesting that the presence of hydrophilic NPs does not affect the adhesion force required to disrupt the interface.[48] Interestingly, at pH 2 the adhesion with NPs increases to 9 ± 2 nN, probably due to the protonation of the carboxylic groups of crude oil that are strongly interacting, forming H-bonded aggregates. Hence, a greater force is required for the retraction of the tip, resulting in an increased adhesion.[67] In summary, when the AFM cantilever pushes against the interface, the only counter force is the interfacial force, which is large in the case of DI water (high IFT value). Creating the additional interface is energetically unfavorable, resulting in a low deformation. Similar arguments can be made with regard to the system at pH 2. As mentioned above, the unfavorable oil−NP interactions prevent NPs from assembling at the interface and keeping the IFT high. As a result, the interface resists the formation of new interfacial area (Figure 3D). At pH 9, the oil−water interface is decorated with NPs that exhibited the lowest IFT, and because in the AFM measurement the counter force is the interfacial force, it results in lower stiffness and the highest deformation.

Dilatational Modulus Experiments and Interfacial Jamming. Studying the response of the interfacial layer to compression and dilatation could provide additional information beyond the IFT measurements. Specifically, it can provide

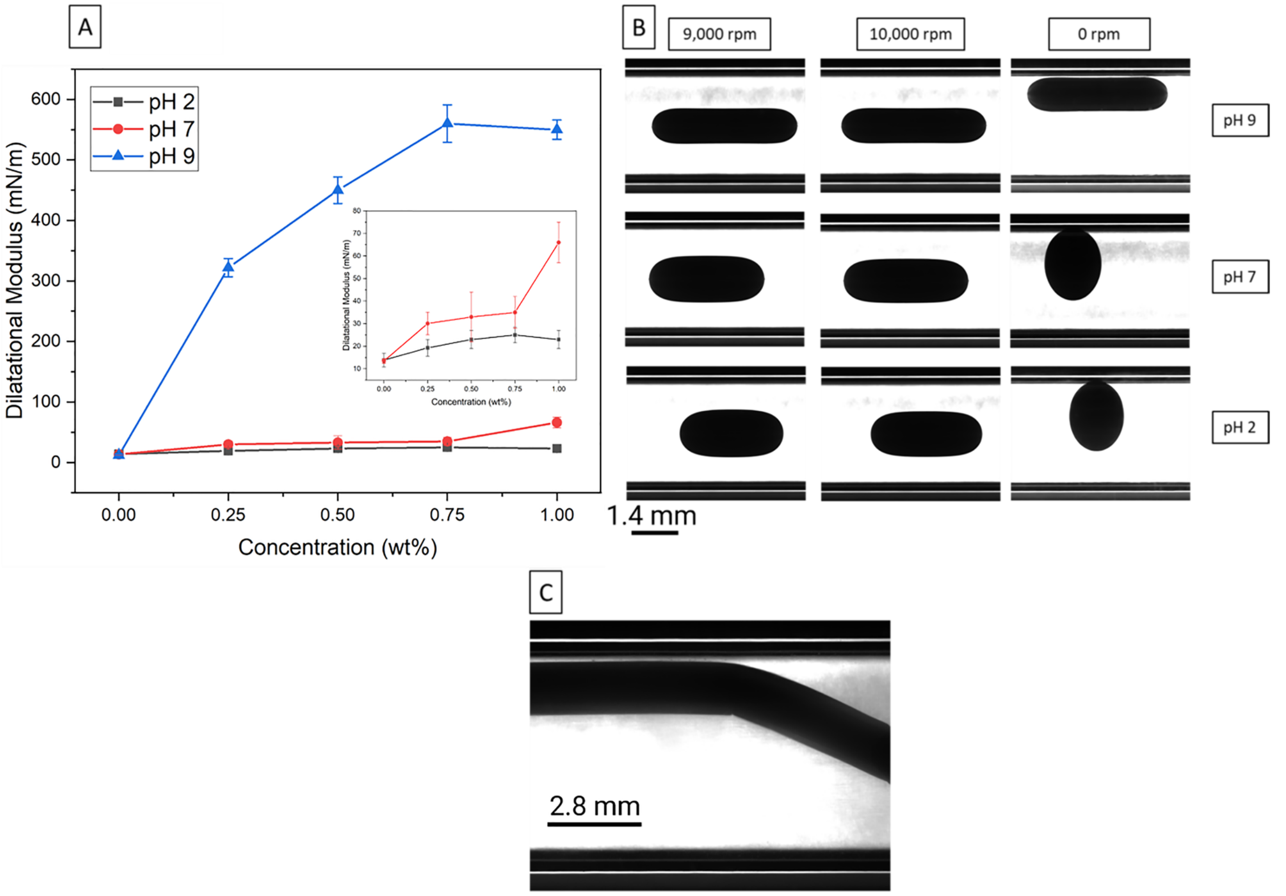

Figure 5. (A) Dilatational modulus of the oil−water interface as a function of the concentration of NPs at different pHs: 2 (black), 7 (red), and 9 (blue). (B) Response of an oil droplet to various numbers of revolutions per minute in the presence of 1 wt % NPs. As noted, at pH 9 the oil droplet remained deformed, when the system was returned to rest (0 rpm). In contrast, it becomes spherical at pH 2 and 7. (C) Demonstration of the highly elastic oil droplet at 0 rpm at pH 9, where the oil droplet can be molded into distinct shapes.

information regarding how the particles are assembled at the interface and the "strength" of the interfacial layer.[68,69] Figure 5A shows the equilibrium dilatational modulus at different pHs. At pH 2, there are no significant changes to the interfacial modulus from that in pure water, irrespective of the concentration used. This is expected because the particle−oil interactions are repulsive and virtually no NPs assemble at the interface. At pH 7, the dilatational modulus exhibited only a modest increase (∼10 mN/m) from that at pH 2 to reach a maximum of 66 mN/m at 1 wt %. In contrast, at pH 9, the modulus increases significantly and reaches 550 mN/m at 1 wt % NPs. We attribute the significant increase at pH 9 to the formation of a closed-packed assembly of the particles at the interface enabled by favorable interparticle and particle−oil interactions (still an attractive interaction with the oil but weakened intraparticle repulsion due to the lower charge because of the deprotonated amines). Dynamic dilatational modulus measurements in which the sinusoidal perturbation of the oil droplet was commenced before the IFT reaches equilibrium provide further insights. The modulus shows a time-dependent behavior for pH 7 and 9 (with a stronger dependency for the latter). In contrast, the dynamic modulus is virtually independent of time at pH 2 (Figure S4). The time-dependent behavior is attributed to the time necessary for the NPs to assemble at the interface.[70]

Particle adsorption at the interface can result in the long-term stability of non-equilibrium shapes of oil droplets. Specifically, interfacial jamming results in arresting any IFT-driven morphological changes of the oil droplets in water.[71] Additionally, it could circumvent the coalescence of oil droplets. Figure 5B shows the oil droplet response at different rotational speeds. As a result of the preferential interfacial adsorption and assembly at pH 9, the oil droplet is arrested and permanently deformed regardless of the number of revolutions per minute, even when the system is returned to rest (0 rpm). The droplet maintains this non-equilibrium shape indefinitely and does not revert to the equilibrium, spherical shape, when rotation ceases. This effect was seen for all systems at pH 9 regardless of the concentration of the NPs in the aqueous phase. In contrast, at pH 2 or 7, the oil droplet reverts to the equilibrium spherical shape at rest. Moreover, the highly elastic oil droplet at pH 9 can be "molded" into shapes, which could be used for applications such as three-dimensional printing.[70] As shown in Figure 5C, the oil droplet was used to create an arc-like shape for the oil−water mixture at pH 9.

The results presented above suggest a behavior consistent with slowing or even preventing the coalescence of oil droplets in the emulsion. As shown in videos that can be accessed via the Supporting Information, when two oil droplets are pushed against each other with a force equal to 15 mN (rotational and gravitational forces), the droplets do not coalesce, when the system is at pH 9. However, coalescence does takes place at pH 2 or 7. Similarly, when the emulsions are subjected to 120$\vec{g}$, they demonstrate different behavior depending on the pH. At

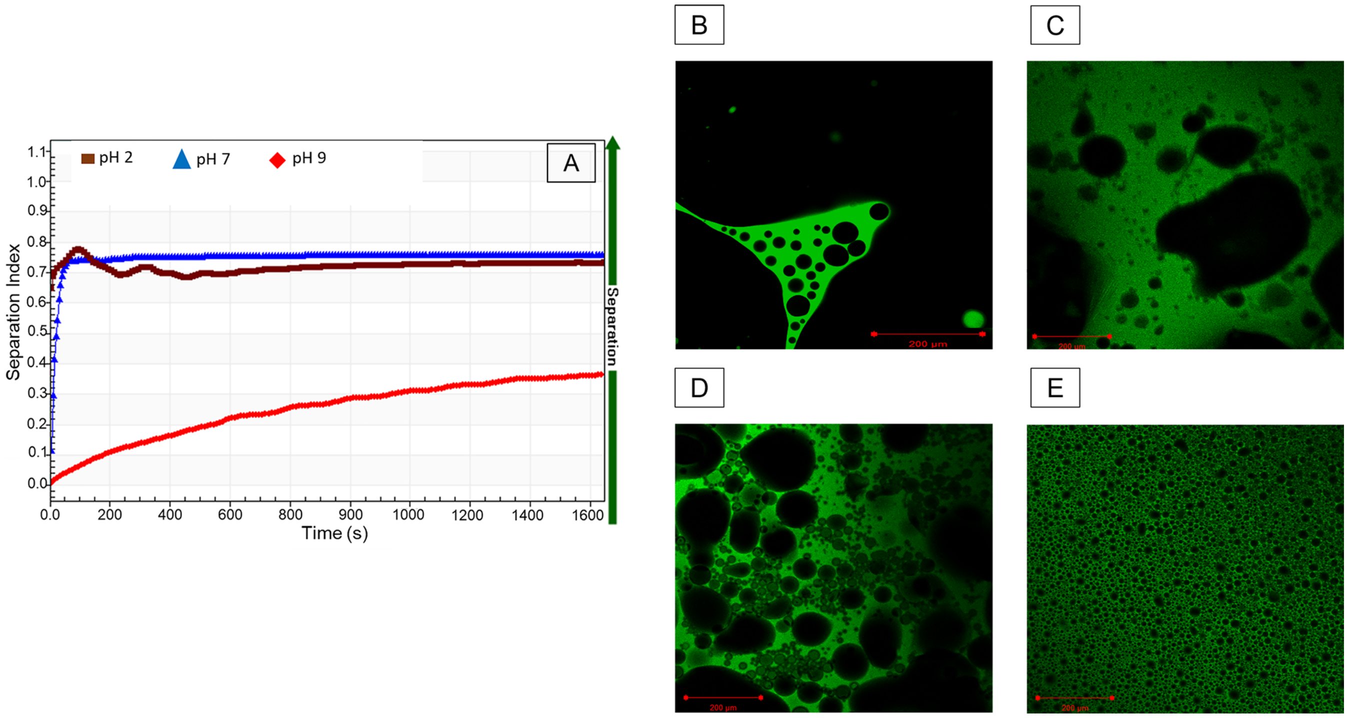

Figure 6. (A) Separation kinetics for the accelerated test of oil−water emulsions at different pHs. Confocal microscopy images of oil (green) and water (black) in water-in-oil emulsions (B) in the absence of NPs and in the presence of 1 wt % NPs at (C) pH 2, (D) pH 7, and (E) pH 9. The scale bar is 200 um.

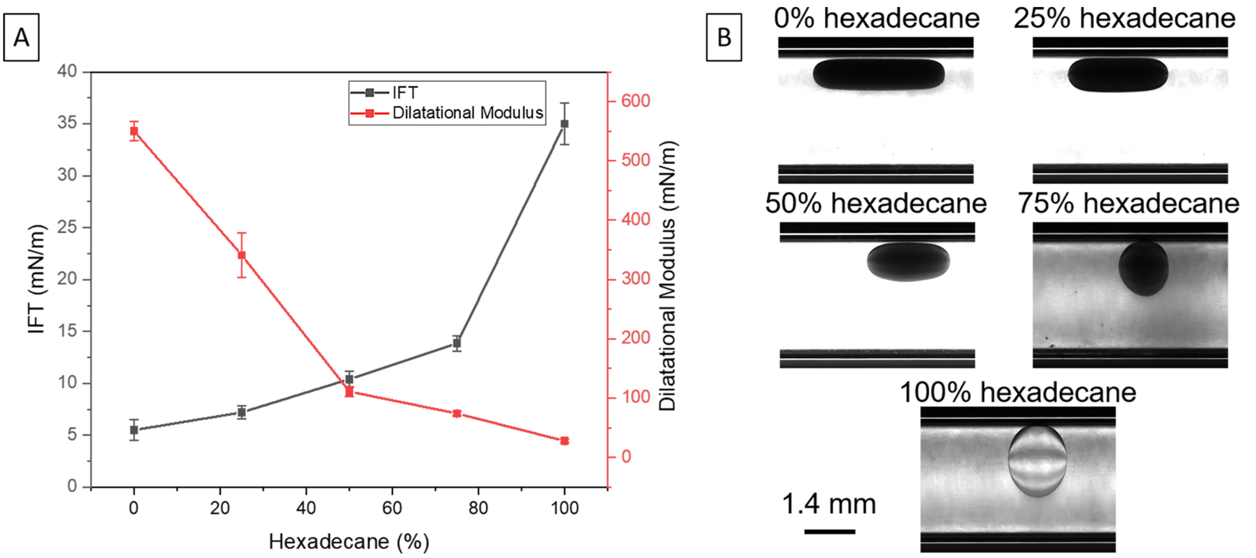

Figure 7. (A) IFT and dilatational modulus of neat crude oil, neat hexadecane, and their mixtures at pH 9 in the presence of 1 wt % silica NPs. (B) Oil droplet behavior at rest of the same.

pH 2 or 7, an immediate phase separation takes place, indicating poor emulsion stability as shown from the fast increase in the separation index (Figure 6A). However, at pH 9, the separation takes place at a much slower rate and does not proceed to completion even under these accelerated test conditions. At pH 9, the separation index at the end of the experiment is ∼0.4 (1 indicates maximum phase separation). In contrast, at pH 2 or 7 the emulsion phase separates quickly and the value reaches 0.75. In contrast to the slow separation for pH 9, at pH 2 or 7, the separation index jumps to 0.7 quickly before it reaches a plateau. At pH 9, the particle−oil interactions are strong, and the particles are strongly attracted to the interface. At the same time, their lower positive charges mediate the interparticle repulsive interactions. The net result is that the particles form a densely packed layer at the interface, which prevents coalescence of the oil droplets. At pH 7, the particle−oil interactions are favorable but the interparticle interactions are strongly repulsive. The net result is a less dense nanoparticle layer at the interface, which fails to prevent the coalescence of the oil droplets.

Confocal microscopy adds further insights into the formation and stability of the emulsions in the presence of NPs. Because of the quick phase separation, it is difficult to unequivocally suggest that the emulsions at pH 2 and 7 (Figure

6C,D) are much more stable than the system in the absence of NPs [pH 7 (Figure 6B)]. In contrast, at pH 9 (Figure. 6E), where the attraction is the strongest and the NP assembly is denser, a highly stable emulsion is formed, which remains unchanged for a long time. These results are consistent with the AFM images (Figure S5). At pH 9, the particles form a dense, closed-packed assembly (Figure S5A). At pH 7, the NPs at the interface are less dense at the interface (Figure S5B). Finally, at pH 2, the interface seems to be almost void of NPs (Figure S5C).

The assembly (jamming) is reversible and can be controlled by inducing a pH change in the system. In one experiment, two oil droplets were released in the capillary tube at pH 9 while 1 wt % NPs were added to the aqueous phase. As shown in Figure S6A, after being spun in the tensiometer for 26 min, the oil droplets remained deformed even at rest. When the pH of the system was decreased to 2, the oil droplets became spherical immediately (Figure S6B).

Furthermore, we examined the behavior of pure hexadecane (as well as mixtures of hexadecane and crude oil) and compared it to that of neat crude oil. The motivation was to control the amount of polar groups in oil as hexadecane does not possess any polar groups. The behavior of hexadecane and that of mixtures of hexadecane and crude oil in the presence of 1 wt % NPs at pH 9 are shown in Figure 7 and summarized in Table 1. The IFT was reduced significantly from that of pure hexadecane (35 mN/m) to 15 mN/m for 75% hexadecane, reaching a value of 5.5 mN/m for 100% crude oil. The surface area increased from 5% for hexadecane to 20% for 100% crude oil. This increase in surface area, because of a greater number of particles adsorbed at the interface, resulted in a significantly higher dilatational modulus as the concentration of crude oil increased. Consistent with the dilatational modulus trends, the oil droplet remained deformed for 50 and 75 vol % crude oil (similar to the 100% crude oil as we discussed above), when returned to rest at the end of the experiment. However, when the concentration of crude oil was reduced to 25 vol % (75% hexadecane), the oil droplet returned to its equilibrium spherical shape (Figure 7B). Similar behavior was observed for pure hexadecane. The number of binding sites, represented by the [COO^-] groups, is decreased upon addition of hexadecane. This, in turn, results in a higher IFT, which leads to a lower modulus. Therefore, although the interparticle interactions are important and are present regardless of the type of oil used, electrostatic interactions between the oil and the NPs play a significant role and both have to work synergistically. Additionally, while hexadecane in water develops a significant amount of negative charge on its surface due to the adsorption of hydroxyl groups, these sites are not sufficient for NPs to be attracted and assemble at the interface, which leaves the properties of the hexadecane−water mixture to be very similar regardless of whether NPs were present.

Table 1. Summary of the IFTs and Dilatational Moduli for Pure Hexadecane and Pure Crude Oil with and without NPs at pH 9

system	IFT (mN/m)	dilatational modulus (mN/m)
hexadecane−water	53.1 ± 3	∼0
crude oil−water	31.4 ± 1	12 ± 2
hexadecane−water−1 wt % SiO_2^+	35.1 ± 2	28 ± 3
crude oil−water−1 wt % SiO_2^+	5.5 ± 1	550 ± 16

For comparison, we have synthesized positively charged silica NPs with the same surface chemistry but using particles with a core diameter of 4 nm. Figure S7 compares the ζ potentials for the 4 and 13 nm NPs at pH 9. The average ζ potentials at pH 9 were 15 and 22 mV for the 4 and 13 nm particles, respectively, although the charge distribution of the 4 nm particles is much narrower. We attribute the narrower charge distribution of the 4 nm particles to their much more homogeneous size distribution. The equilibrium IFT for an oil−water mixture containing 1 wt % NPs is 6.2 mN/m, for the silica NPs based on the 4 nm cores. The corresponding value for the 13 nm cores is 5.5 mN/m (Figure S8A). The steeper decrease as a function of time for the 4 nm NPs may be due to the faster diffusion to the interface of the smaller NPs allowing the system to reach the equilibrium IFT in a shorter time. However, adsorption of the smaller particles is energetically less favorable (eqs 1 and 2), leading to an equilibrium dilatational modulus for the 4 nm particles an order of magnitude lower than that of the particles based on the 13 nm cores. Additionally, the oil droplet does maintain its elongated shape after the system is returned to rest following deformation (Figure S8B).

Lastly, we compare the behavior of the positively charged NPs to those of positively charged molecular surfactants. Three different concentrations of CTAB were tested at pH 9, where we see the largest changes with the NPs: below the critical micelle concentration (CMC), at the CMC, and above the CMC (the CMC of CTAB is 0.9 mM).[72,73] For the concentrations tested, CTAB results in an IFT of <1 mN/m, which is an order of magnitude lower than that of the NPs. The dilatational modulus was significantly lower (<10 mN/m), even lower than that of the pure oil−water interface as expected for molecular surfactants.[51] Consistent with the results presented above, the oil droplet did not reach a jamming state at all concentrations tested and did not remain deformed when the system was returned to rest.

■ CONCLUSIONS

We have combined macroscopic and microscopic techniques to elucidate the assembly and its response to pH using positively charged silica nanoparticles in crude oil−water emulsions. The particles were functionalized with a mixture of silanes containing primary, secondary, and quaternary amines. The quaternary ammonium groups are permanently charged, while the primary and secondary amine groups induce pH-dependent behavior. This feature allows for the interfacial properties to be fine-tuned by varying the pH of the system. The interfacial assembly and, therefore, the interfacial properties were governed mainly by the particle−oil and particle−particle interactions. At pH 2, at which the particles and oil were positively charged and, thus, virtually absent from the interface, the IFT decreased slightly, and the dilatational modulus was similar to that of a pure water−oil emulsion. In contrast, at pH 9, the particle−oil attractive interactions are maximized and the interparticle repulsion decreases leading to a dense NP assembly. As a result, the IFT is reduced to 5.5 mN/m and the dilatational modulus increased to 550 mN/m. At pH 9, the particle−oil attractive interactions are maximized and the interparticle repulsion is optimal. Under these conditions, the IFT is reduced to 5.5 mN/m and the dilatational modulus increased to 550 mN/m. At an intermediate pH (7), the attraction of the NPs to the oil is maximized but so are the repulsive interactions between the NPs leading to a less dense assembly. The net result is both the IFT and the dilatational modulus are more comparable to those of the system at pH 2.

The assembly at pH 9 resulted in a solid-like interface with the oil droplet deformed permanently. As a result, when two oil droplets were pushed against each other, they did not coalesce. The macroscopic observations were supported microscopically by the AFM results in which the stiffness and resistance to form the interface were lowest for pH 9 and highest for pH 2. Imaging of the interface indicated the presence of closely packed NPs and maximum coverage at pH 9, lower coverage at pH 7 with the particles being apart, and virtually no particles pH 2. NPs with a smaller particle size and essentially the same ζ potential and surface chemistry lead to a similar equilibrium IFT, although the smaller particles reach the plateau much faster. In addition, the dilatational modulus was an order of magnitude lower for the smaller NPs and the system did not reach a jammed state. Lastly, we compared the behavior of the NPs to that of molecular surfactants. Molecular surfactants result in an IFT an order of magnitude lower than in the case of the NPs but a low dilatational modulus (even lower than in the pristine oil−water system). In both cases for the smaller NPs and the CTAB surfactants, the oil droplet returns to the spherical equilibrium shape when the system is returned to rest. Altogether, this study has identified important aspects contributing to the NP assembly, interfacial properties, and macroscopic behavior of oil−water emulsions. The new mechanistic understanding coupled with the colloidal stability of the surface-modified silica NPs under realistic conditions might pave the way for a series of practical applications in the chemical, environmental, food, and pharmaceutical fields.

■ ASSOCIATED CONTENT

Supporting Information

The Supporting Information is available free of charge at https://pubs.acs.org/doi/10.1021/acs.langmuir.2c03286.

> Supporting figures of the method used to calculate the complex dilatational modulus, the ζ potential for the modified and unmodified silica NPs, and the ζ potential of the particles with different sizes; FT-IR spectrum of crude oil and hexadecane with 1 wt % stearic acid; dynamic dilatational modulus for the NP suspension at different pHs; videos of the coalescence of oil droplets at pH 2 and 7 and stability at pH 9; AFM images of the interface decorated with NPs; controlling the assembly of the NP at the interface and the behavior of the oil droplets by changing the pH of the aqueous phase; and comparison of the results of the IFT and dilatational modulus for the 13 and 4 nm modified NPs (PDF)

■ AUTHOR INFORMATION

Corresponding Author

Emmanuel P. Giannelis − *Department of Materials Science and Engineering, Cornell University, Ithaca, New York 14850, United States*; Email: epg2@cornell.edu

Authors

Ahmed Wasel Alsmaeil − *Robert Frederick Smith School of Chemical and Biomolecular Engineering, Cornell University, Ithaca, New York 14850, United States; EXPEC Advanced Research Center, Saudi Aramco, Dhahran 31261, Saudi Arabia*; orcid.org/0000-0001-7121-9876

Antonios Kouloumpis − *Department of Materials Science and Engineering, Cornell University, Ithaca, New York 14850, United States*; orcid.org/0000-0002-8738-3141

Georgia Potsi − *Department of Materials Science and Engineering, Cornell University, Ithaca, New York 14850, United States*; orcid.org/0000-0001-5121-0866

Mohamed Amen Hammami − *Department of Materials Science and Engineering, Cornell University, Ithaca, New York 14850, United States*; orcid.org/0000-0002-6162-3629

Mazen Yousef Kanj − *College of Petroleum Engineering & Geosciences, King Fahd University of Petroleum & Minerals, Dhahran 31261, Saudi Arabia*; orcid.org/0000-0002-2674-4505

Complete contact information is available at: https://pubs.acs.org/10.1021/acs.langmuir.2c03286

Author Contributions

A.W.A. conducted the experiments and wrote the draft of the manuscript. A.K. helped with the synthesis and performed the AFM experiments. G.P. helped with the synthesis and performed the XPS experiment. M.A.H. helped with the synthesis and conducted the confocal microscopy experiments. M.Y.K. offered guidance about the research. E.P.G. guided the work and recommended experiments. All authors discussed and commented on the manuscript.

Notes

The authors declare no competing financial interest.

■ ACKNOWLEDGMENTS

A.W.A. acknowledges Saudi Aramco for the graduate scholarship under the Aramco Young Researchers scholarship. The authors appreciate Dr. Genggeng Qi for his help with the synthesis procedure. The authors appreciate Mohammed Alshammasi for his support in coding. The authors appreciate Andrew Galvin for his help with the CTAB IFT experiments. The authors acknowledge Bashayer Aldakkan for her help with the confocal microscopy images. The work made use of the Cornell Center for Materials Research Shared Facilities, which are supported by the National Science Foundation MRSEC program (DMR-1719875). Imaging data were acquired through the Cornell Institute of Biotechnology's Imaging Facility, with National Institutes of Health Grant 1S10OD010605 funding for the shared Andor Revolution Spinning Disk Confocal Microscope. bioRender was utilized to create some of the illustrations in the manuscript. This publication is based on work supported by the College of Petroleum Engineering and Geosciences, King Fahd University of Petroleum and Minerals.

■ REFERENCES

(1) Maestro, A.; Deshmukh, O. S.; Mugele, F.; Langevin, D. Interfacial Assembly of Surfactant-Decorated Nanoparticles: On the Rheological Description of a Colloidal 2D Glass. *Langmuir* **2015**, *31* (23), 6289−6297.

(2) Fang, Z.; Cao, X.-R.; Yu, Y.-L.; Li, M. Fabrication and Characterization of Microcapsule Encapsulating EOR Surfactants by Microfluidic Technique. *Colloids Surf., A* **2019**, *570*, 282−292.

(3) Yano, H.; Fukui, A.; Kajiwara, K.; Kobayashi, I.; Yoza, K.; Satake, A.; Villeneuve, M. Development of Gluten-Free Rice Bread: Pickering

Stabilization as a Possible Batter-Swelling Mechanism. *LWT-Food Sci. Technol.* **2017**, *79*, 632−639.

(4) Putro, J. N.; Ismadji, S.; Gunarto, C.; Soetaredjo, F. E.; Ju, Y. H. A Study of Anionic, Cationic, and Nonionic Surfactants Modified Starch Nanoparticles for Hydrophobic Drug Loading and Release. *J. Mol. Liq.* **2020**, *298*, 112034.

(5) Wu, B.; Yang, C.; Li, B.; Feng, L.; Hai, M.; Zhao, C.-X.; Chen, D.; Liu, K.; Weitz, D. A. Active Encapsulation in Biocompatible Nanocapsules. *Small* **2020**, *16* (30), 2002716.

(6) Borji, H.; Ayoub, G. M.; Al-Hindi, M.; Malaeb, L.; Hamdan, H. Z. Nanotechnology to Remove Polychlorinated Biphenyls and Polycyclic Aromatic Hydrocarbons from Water: A Review. *Environ. Chem. Lett.* **2020**, *18* (3), 729−746.

(7) Ojo, O. F.; Farinmade, A.; Trout, J.; Omarova, M.; He, J.; John, V.; Blake, D. A.; Lvov, Y. M.; Zhang, D.; Nguyen, D.; Bose, A. Stoppers and Skins on Clay Nanotubes Help Stabilize Oil-in-Water Emulsions and Modulate the Release of Encapsulated Surfactants. *ACS Appl. Nano Mater.* **2019**, *2* (6), 3490−3500.

(8) Farinmade, A.; Ojo, O. F.; Trout, J.; He, J.; John, V.; Blake, D. A.; Lvov, Y. M.; Zhang, D.; Nguyen, D.; Bose, A. Targeted and Stimulus-Responsive Delivery of Surfactant to the Oil-Water Interface for Applications in Oil Spill Remediation. *ACS Appl. Mater. Interfaces* **2020**, *12* (1), 1840−1849.

(9) Hammami, M. A.; Kanj, M. Y.; Giannelis, E. P. Monitoring the Early Stages of Formation of Oil-Water Emulsions Using Flow Cytometry. *Langmuir* **2022**, *38* (1), 62−71.

(10) Aldakkan, B. S.; Hammami, M. A.; Qi, G.; Kanj, M. Y.; Giannelis, E. P. Stimuli-Responsive, Hydrolyzable Poly(Vinyl Laurate-Co-Vinyl Acetate) Nanoparticle Platform for In Situ Release of Surfactants. *ACS Appl. Mater. Interfaces* **2021**, *13* (21), 25553−25562.

(11) Kanj, M.; Sakthivel, S.; Giannelis, E. Wettability Alteration in Carbonate Reservoirs by Carbon Nanofluids. *Colloids Surf., A* **2020**, *598*, 124819.

(12) Mohammed, S.; Kuzmenko, I.; Gadikota, G. Reversible Assembly of Silica Nanoparticles at Water-Hydrocarbon Interfaces Controlled by SDS Surfactant. *Nanoscale* **2021**, *14* (1), 127−139.

(13) Alsmaeil, A. W.; Hammami, M. A.; Enotiadis, A.; Kanj, M. Y.; Giannelis, E. P. Encapsulation of an Anionic Surfactant into Hollow Spherical Nanosized Capsules: Size Control, Slow Release, and Potential Use for Enhanced Oil Recovery Applications and Environmental Remediation. *ACS Omega* **2021**, *6* (8), 5689−5697.

(14) Qu, M.; Hou, J.; Liang, T.; Qi, P. Amphiphilic Rhamnolipid Molybdenum Disulfide Nanosheets for Oil Recovery. *ACS Appl. Nano Mater.* **2021**, *4* (3), 2963−2972.

(15) Cain, J. D.; Azizi, A.; Maleski, K.; Anasori, B.; Glazer, E. C.; Kim, P. Y.; Gogotsi, Y.; Helms, B. A.; Russell, T. P.; Zettl, A. Sculpting Liquids with Two-Dimensional Materials: The Assembly of Ti3C2Tx MXene Sheets at Liquid-Liquid Interfaces. *ACS Nano* **2019**, *13* (11), 12385−12392.

(16) Noskov, B. A.; Bykov, A. G. Dilational Rheology of Monolayers of Nano- and Micropaticles at the Liquid-Fluid Interfaces. *Curr. Opin. Colloid Interface Sci.* **2018**, *37*, 1−12.

(17) Griffith, C.; Daigle, H. Manipulation of Pickering Emulsion Rheology Using Hydrophilically Modified Silica Nanoparticles in Brine. *J. Colloid Interface Sci.* **2018**, *509*, 132−139.

(18) Vialetto, J.; Camerin, F.; Grillo, F.; Ramakrishna, S. N.; Rovigatti, L.; Zaccarelli, E.; Isa, L. Effect of Internal Architecture on the Assembly of Soft Particles at Fluid Interfaces. *ACS Nano* **2021**, *15* (8), 13105−13117.

(19) Stehl, D.; Skale, T.; Hohl, L.; Lvov, Y.; Koetz, J.; Kraume, M.; Drews, A.; von Klitzing, R. Oil-in-Water Pickering Emulsions Stabilized by Halloysite Clay Nanotubes Toward Efficient Filterability. *ACS Appl. Nano Mater.* **2020**, *3* (12), 11743−11751.

(20) Feng, T.; Hoagland, D. A.; Russell, T. P. Interfacial Rheology of Polymer/Carbon Nanotube Films Co-Assembled at the Oil/Water Interface. *Soft Matter* **2016**, *12* (42), 8701−8709.

(21) Yi, D.; Jeong, G.; Seo, J.-H.; Yoo, M. J.; Yang, H. Carbon Dots with Tailored Surface Wettability as Pickering Emulsifiers. *ACS Appl. Nano Mater.* **2022**, *5* (8), 10258−10267.

(22) Tan, C.; Zhao, P.; Zhou, Y.; Liu, M. Hydrophobic Halloysite Nanotubes via Ball Milling for Stable Pickering Emulsions: Implications for Food Preservation. *ACS Appl. Nano Mater.* **2022**, *5* (8), 11289−11301.

(23) Kutuzov, S.; He, J.; Tangirala, R.; Emrick, T.; Russell, T. P.; Böker, A. On the Kinetics of Nanoparticle Self-Assembly at Liquid/Liquid Interfaces. *Phys. Chem. Chem. Phys.* **2007**, *9* (48), 6351−6358.

(24) Larson-Smith, K.; Jackson, A.; Pozzo, D. C. SANS and SAXS Analysis of Charged Nanoparticle Adsorption at Oil-Water Interfaces. *Langmuir* **2012**, *28* (5), 2493−2501.

(25) Hua, X.; Bevan, M. A.; Frechette, J. Competitive Adsorption between Nanoparticles and Surface Active Ions for the Oil-Water Interface. *Langmuir* **2018**, *34* (16), 4830−4842.

(26) Bizmark, N.; Ioannidis, M. A.; Henneke, D. E. Irreversible Adsorption-Driven Assembly of Nanoparticles at Fluid Interfaces Revealed by a Dynamic Surface Tension Probe. *Langmuir* **2014**, *30* (3), 710−717.

(27) Israelachvili, J. N. 4 - Interactions Involving Polar Molecules. In *Intermolecular and Surface Forces*, 3rd ed.; Israelachvili, J. N., Ed.; Academic Press: San Diego, 2011; pp 71−90.

(28) Sun, Z.; Yan, X.; Xiao, Y.; Hu, L.; Eggersdorfer, M.; Chen, D.; Yang, Z.; Weitz, D. A. Pickering Emulsions Stabilized by Colloidal Surfactants: Role of Solid Particles. *Particuology* **2022**, *64*, 153−163.

(29) Shi, S.; Russell, T. P. Nanoparticle Assembly at Liquid-Liquid Interfaces: From the Nanoscale to Mesoscale. *Adv. Mater. (Weinheim, Ger.)* **2018**, *30* (44), 1800714.

(30) Lin, Y.; Skaff, H.; Emrick, T.; Dinsmore, A. D.; Russell, T. P. Nanoparticle Assembly and Transport at Liquid-Liquid Interfaces. *Science* **2003**, *299* (5604), 226−229.

(31) Hua, X.; Bevan, M. A.; Frechette, J. Reversible Partitioning of Nanoparticles at an Oil-Water Interface. *Langmuir* **2016**, *32* (44), 11341−11352.

(32) Whitby, C. P.; Djerdjev, A. M.; Beattie, J. K.; Warr, G. G. Nanoparticle Adsorption and Stabilisation of Surfactant-Free Emulsions. *J. Colloid Interface Sci.* **2006**, *301* (1), 342−345.

(33) Biswal, N. R.; Rangera, N.; Singh, J. K. Effect of Different Surfactants on the Interfacial Behavior of the *n* -Hexane-Water System in the Presence of Silica Nanoparticles. *J. Phys. Chem. B* **2016**, *120* (29), 7265−7274.

(34) Saien, J.; Fadaei, V. The Study of Interfacial Tension of Kerosene-Water under Influence of CTAB Surfactant and Different Size Silica Nanoparticles. *J. Mol. Liq.* **2018**, *255*, 439−446.

(35) Calzolari, D. C. E.; Pontoni, D.; Deutsch, M.; Reichert, H.; Daillant, J. Nanoscale Structure of Surfactant-Induced Nanoparticle Monolayers at the Oil-Water Interface. *Soft Matter* **2012**, *8* (45), 11478−11483.

(36) Metin, C. O.; Baran, J. R.; Nguyen, Q. P. Adsorption of Surface Functionalized Silica Nanoparticles onto Mineral Surfaces and Decane/Water Interface. *J. Nanopart. Res.* **2012**, *14* (11), 1246.

(37) Anjali, T. G.; Basavaraj, M. G. General Destabilization Mechanism of PH-Responsive Pickering Emulsions. *Phys. Chem. Chem. Phys.* **2017**, *19* (45), 30790−30797.

(38) Chai, Y.; Lukito, A.; Jiang, Y.; Ashby, P. D.; Russell, T. P. Fine-Tuning Nanoparticle Packing at Water-Oil Interfaces Using Ionic Strength. *Nano Lett.* **2017**, *17* (10), 6453−6457.

(39) Xu, H.-N.; Li, Y.-H.; Zhang, L. Driving Forces for Accumulation of Cellulose Nanofibrils at the Oil/Water Interface. *Langmuir* **2018**, *34* (36), 10757−10763.

(40) Toor, A.; Forth, J.; Bochner de Araujo, S.; Merola, M. C.; Jiang, Y.; Liu, X.; Chai, Y.; Hou, H.; Ashby, P. D.; Fuller, G. G.; Russell, T. P. Mechanical Properties of Solidifying Assemblies of Nanoparticle Surfactants at the Oil-Water Interface. *Langmuir* **2019**, *35* (41), 13340−13350.

(41) Huang, C.; Cui, M.; Sun, Z.; Liu, F.; Helms, B. A.; Russell, T. P. Self-Regulated Nanoparticle Assembly at Liquid/Liquid Interfaces: A Route to Adaptive Structuring of Liquids. *Langmuir* **2017**, *33* (32), 7994−8001.

https://doi.org/10.1021/acs.langmuir.2c03286

(42) Cui, M.; Emrick, T.; Russell, T. P. Stabilizing Liquid Drops in Nonequilibrium Shapes by the Interfacial Jamming of Nanoparticles. *Science* **2013**, *342* (6157), 460−463.

(43) Sun, Z.; Feng, T.; Russell, T. P. Assembly of Graphene Oxide at Water/Oil Interfaces: Tessellated Nanotiles. *Langmuir* **2013**, *29* (44), 13407−13413.

(44) Li, W.; Leong, T. S. H.; Ashokkumar, M.; Martin, G. J. O. A Study of the Effectiveness and Energy Efficiency of Ultrasonic Emulsification. *Phys. Chem. Chem. Phys.* **2018**, *20* (1), 86−96.

(45) Thompson, K. L.; Derry, M. J.; Hatton, F. L.; Armes, S. P. Long-Term Stability of n-Alkane-in-Water Pickering Nanoemulsions: Effect of Aqueous Solubility of Droplet Phase on Ostwald Ripening. *Langmuir* **2018**, *34* (31), 9289−9297.

(46) Detloff, T.; Sobisch, T.; Lerche, D. Particle Size Distribution by Space or Time Dependent Extinction Profiles Obtained by Analytical Centrifugation (Concentrated Systems). *Powder Technol.* **2007**, *174* (1), 50−55.

(47) Wang, B.; Tian, H.; Xiang, D. Stabilizing the Oil-in-Water Emulsions Using the Mixtures of Dendrobium Officinale Polysaccharides and Gum Arabic or Propylene Glycol Alginate. *Molecules* **2020**, *25* (3), 759.

(48) Almorihil, J.; Alsmaeil, A.; Kaidar, Z.; AlSofi, A. Produced Water Quality: Uncovering the Effects of Centrifugation for Water and Chemical Floods Using a Dispersion Analyzer. SPE/IATMI Asia Pacific Oil & Gas Conference and Exhibition, Virtual, October 2021; SPE-205534-MS.

(49) Yerramilli, M.; Ghosh, S. Long-Term Stability of Sodium Caseinate-Stabilized Nanoemulsions. *J. Food Sci. Technol.* **2017**, *54* (1), 82−92.

(50) Viades-Trejo, J.; Gracia-Fadrique, J. Spinning Drop Method: From Young-Laplace to Vonnegut. *Colloids Surf., A* **2007**, *302* (1), 549−552.

(51) Zamora, J. M.; Marquez, R.; Forgiarini, A. M.; Langevin, D.; Salager, J.-L. Interfacial Rheology of Low Interfacial Tension Systems Using a New Oscillating Spinning Drop Method. *J. Colloid Interface Sci.* **2018**, *519*, 27−37.

(52) Kuznicki, N. P.; Harbottle, D.; Masliyah, J. H.; Xu, Z. Probing Mechanical Properties of Water-Crude Oil Interfaces and Colloidal Interactions of Petroleum Emulsions Using Atomic Force Microscopy. *Energy Fuels* **2017**, *31* (4), 3445−3453.

(53) Vialetto, J.; Nussbaum, N.; Bergfreund, J.; Fischer, P.; Isa, L. Influence of the Interfacial Tension on the Microstructural and Mechanical Properties of Microgels at Fluid Interfaces. *J. Colloid Interface Sci.* **2022**, *608*, 2584−2592.

(54) Yan, F.; Spyrou, K.; Thomou, E.; Kumar, S.; Cao, H.; Stuart, M. C. A.; Pei, Y.; Gournis, D.; Rudolf, P. Smectite Clay Pillared with Copper Complexed Polyhedral Oligosilsesquioxane for Adsorption of Chloridazon and Its Metabolites. *Environ. Sci.: Nano* **2020**, *7* (2), 424−436.

(55) Ravi, S.; Zhang, S.; Lee, Y.-R.; Kang, K.-K.; Kim, J.-M.; Ahn, J.-W.; Ahn, W.-S. EDTA-Functionalized KCC-1 and KIT-6 Mesoporous Silicas for Nd3+ Ion Recovery from Aqueous Solutions. *J. Ind. Eng. Chem.* **2018**, *67*, 210−218.

(56) Marras, A. E.; Vieregg, J. R.; Ting, J. M.; Rubien, J. D.; Tirrell, M. V. Polyelectrolyte Complexation of Oligonucleotides by Charged Hydrophobic—Neutral Hydrophilic Block Copolymers. *Polymers* **2019**, *11* (1), 83.

(57) Wang, S.; Song, H.; Ong, W. Y.; Han, M. Y.; Huang, D. Positively Charged and PH Self-Buffering Quantum Dots for Efficient Cellular Uptake by Charge Mediation and Monitoring Cell Membrane Permeability. *Nanotechnology* **2009**, *20* (42), 425102.

(58) Surface Forces. In *Physics and Chemistry of Interfaces*; John Wiley & Sons, Ltd., 2003; pp 80−117. DOI: 10.1002/3527602313.ch6

(59) Metin, C. O.; Lake, L. W.; Miranda, C. R.; Nguyen, Q. P. Stability of Aqueous Silica Nanoparticle Dispersions. *J. Nanopart. Res.* **2011**, *13* (2), 839−850.

(60) Parisotto, G.; Ferrão, M. F.; Müller, A. L. H.; Müller, E. I.; Santos, M. F. P.; Guimarães, R. C. L.; Dias, J. C. M.; Flores, É. M. M. Total Acid Number Determination in Residues of Crude Oil Distillation Using ATR-FTIR and Variable Selection by Chemometric Methods. *Energy Fuels* **2010**, *24* (10), 5474−5478.

(61) Samanta, A.; Ojha, K.; Mandal, A. Interactions between Acidic Crude Oil and Alkali and Their Effects on Enhanced Oil Recovery. *Energy Fuels* **2011**, *25* (4), 1642−1649.

(62) Vysotsky, Y. B.; Kartashynska, E. S.; Vollhardt, D.; Fainerman, V. B. Surface PKa of Saturated Carboxylic Acids at the Air/Water Interface: A Quantum Chemical Approach. *J. Phys. Chem. C* **2020**, *124* (25), 13809−13818.

(63) Andersen, S. I.; Chandra, M. S.; Chen, J.; Zeng, B. Y.; Zou, F.; Mapolelo, M.; Abdallah, W.; Buiting, J. J. Detection and Impact of Carboxylic Acids at the Crude Oil-Water Interface. *Energy Fuels* **2016**, *30* (6), 4475−4485.

(64) Marinova, K. G.; Alargova, R. G.; Denkov, N. D.; Velev, O. D.; Petsev, D. N.; Ivanov, I. B.; Borwankar, R. P. Charging of Oil-Water Interfaces Due to Spontaneous Adsorption of Hydroxyl Ions. *Langmuir* **1996**, *12* (8), 2045−2051.

(65) *Adsorption Technology in Water Treatment: Fundamentals, Processes, and Modeling*; De Gruyter, 2012; pp 123−168.

(66) McNamee, C. E.; Kappl, M. Forces and Physical Properties of the Langmuir Monolayers of TiO2 Particles at Air/Water Interfaces after Collisions by a Particle in Water. *RSC Adv.* **2016**, *6* (59), 54440−54448.

(67) Kuznicki, N. P.; Harbottle, D.; Masliyah, J.; Xu, Z. Dynamic Interactions between a Silica Sphere and Deformable Interfaces in Organic Solvents Studied by Atomic Force Microscopy. *Langmuir* **2016**, *32* (38), 9797−9806.

(68) Jiang, P.; Zhang, L.; Tang, D.; Li, L.; Ge, J.; Zhang, G.; Pei, H. Effect of Nano-SiO2 and Surfactants on the Oil-Water Interfacial Properties. *Colloid Polym. Sci.* **2019**, *297* (6), 903−915.

(69) Da, C.; Zhang, X.; Alzobaidi, S.; Hu, D.; Wu, P.; Johnston, K. P. Tuning Surface Chemistry and Ionic Strength to Control Nanoparticle Adsorption and Elastic Dilational Modulus at Air-Brine Interface. *Langmuir* **2021**, *37* (19), 5795−5809.

(70) Kamkar, M.; Erfanian, E.; Bazazi, P.; Ghaffarkhah, A.; Sharif, F.; Xie, G.; Kannan, A.; Arjmand, M.; Hejazi, S. H.; Russell, T. P.; Fuller, G. G.; Sundararaj, U. Interfacial Assembly of Graphene Oxide: From Super Elastic Interfaces to Liquid-in-Liquid Printing. *Adv. Mater. Interfaces* **2022**, *9* (6), 2101659.

(71) Jia, X.; Song, J.; Lv, W.; Hill, J. P.; Nakanishi, J.; Ariga, K. Adaptive Liquid Interfaces Induce Neuronal Differentiation of Mesenchymal Stem Cells through Lipid Raft Assembly. *Nat. Commun.* **2022**, *13* (1), 3110.

(72) Alsmaeil, A. W.; Hammami, M. A.; Abdel-Fattah, A. I.; Kanj, M. Y.; Giannelis, E. P. From Biomedical to Oil Industry: Promising Mesoporous Materials for Oil Field Applications. SPE Europec featured 82nd EAGE Conference and Exhibition, Amsterdam, The Netherlands, October 2021; SPE-205175-MS.

(73) Goronja, J.; Janosevic-Lezaic, A.; Dimitrijevic, B.; Malenovic, A.; Stanisavljev, D.; Pejic, N. Determination of Critical Micelle Concentration of Cetyltrimethylammonium Bromide: Different Procedures for Analysis of Experimental Data. *Hem Ind.* **2016**, *70* (4), 485−492.